Active Clamped Dual Current-Fed Bidirectional DC-DC Converter for Wide Voltage Range Applications

Sachin Chauhan, Andrei Blinov, Andrii Chub and Dmitri Vinnikov
Department of Electrical Power Engineering and Mechatronics
Tallinn University of Technology
Tallinn, Estonia
sachin.chauhan@taltech.ee

***Abstract*— This paper presents an active clamped dual current-fed (ACDCF) bidirectional dc-dc converter for the wide voltage range EV charging/discharging operation. This current-fed configuration supports minimizing the input/output current ripples of the converter. This configuration can be implemented as a dc-to-dc interface between different energy sources and storage technologies like supercapacitors, fuel cells, Li-ion batteries, photovoltaic panels, etc. In addition, the current-fed switching cell has been augmented with the active clamp circuits to suppress the turn-off voltage spikes. It helps in reducing the safe operation voltage limit, which eventually results in a selection of relatively low voltage switches with low on-state resistance. Furthermore, the converter is designed to operate in different modes using topology morphing control (TMC). This helps to extend the converter's operating and soft switching ranges. The component selection and converter design are briefly expressed, along with the theoretical assessment. Finally, the features of the proposed converter topology have been verified through simulations.**

Keywords*— *Active clamping, current-fed dc-dc converters, bidirectional power flow, EV charger, topology morphing

I. INTRODUCTION

Power electronic interfaces based on isolated high gain dc-dc topologies have been extensively used and proved effective for applications with a wide voltage variation range [1]. The electric vehicle (EV) chargers are intended to work with a broad spectrum of voltages and sometimes need a bidirectional power flow feature for vehicle-to-grid (V2G) modes [2]. Therefore, the current scenarios need a solution that can cover the overall aspect of EV charging.

The full-bridge topologies have proven to be a universal solution among others (half-bridge and push-pull) and suitable for wide voltage range applications [3]. Li-ion battery chargers often utilize isolated bidirectional high-gain converters, out of which the dual active bridge (DAB) converter is an attractive option among other topologies [4]. It has flexible control algorithms that help in achieving the soft switching condition and low circulating current for a wide range of loads [5], [6], [7]. Apart from typical single-phase DAB converters, a three-phase converter with asymmetric triple-phase magnetics has also been introduced for wide operating range applications [8]. However, this converter needs a dc supply and a capacitor to clamp both the neutral points of the three-phase transformer along with one extra set of switches on both sides compared to the DAB converter.

In [9], the dual pulse with modulation (DPWM) with a decoupled control strategy has been proposed to enhance efficiency for a wide range of conditions. However, this increases the control complexity by employing two compensation loops and one PI controller followed by model predictive control to control a DAB converter [9]. Although [10] used similar three-phase magnetics with buck-based active clamp circuits that minimize the number of active switches, it lacks bidirectional power flow capability and features reduced efficiency compared to galvanically isolated active clamp current-fed converters [11].

In [12], a zero current switching (ZCS) pull-push dc-dc converter has been proposed with a current-fed circuit. This work claims to eliminate the active clamp circuit and provides zero current switching (ZCS) and natural voltage clamping (NVC). At the same time, this work did not consider the wide variation in output voltage, which is essentially a requirement for universal chargers. Reference [13] describes the active clamped zero voltage switching (ZVS) current-fed full-bridge topology. This converter works effectively with high voltage gain but lacks in buck operation mode. Hence, it cannot be fully considered for a wide range of input-output voltage variations and is also limited to unidirectional power flow.

In [14], a current-fed dual active bridge has been presented with improved modulation strategies to control the peak current in the converter using an additional control variable. However, this converter has only been studied for low-voltage high-power applications. In [15], a three-phase current-fed dc-dc converter has been presented with secondary modulation techniques to clamp the switch voltages naturally. It is effective for high gain operations but limited to below unity voltage gain, i.e., buck operation. On the other hand, topology morphing control can be explored with the benefits of current-fed converters, as TMC can substantially extend the range and capabilities of generic topologies [16] - [20].

While considering the EV charging case study, including bidirectional power flow and a broad output voltage range (150-1000 V), this work proposes a dc-dc topology with a minimized number of magnetics required to operate as a current-fed converter in both forward and reverse power flow. The conventional single-side current-fed topology was typically used in low-voltage and low-power applications [4]. Hence, this paper addresses the limitations of the existing literature on current-fed bidirectional converters by adopting the best-suited combination of modulation schemes along with topology morphing control in the proposed topology. The key contribution of this work is in analyzing the proposed converter topology, comparing it with the conventional topologies in terms of the components' current and voltage

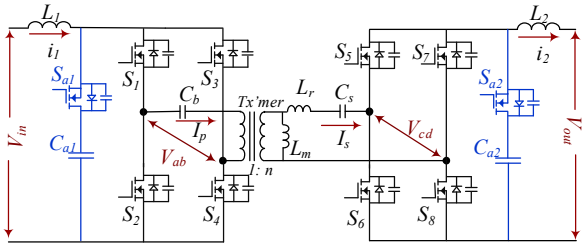

Fig. 1. Operating modes with current/voltage-fed configuration topology morphing.

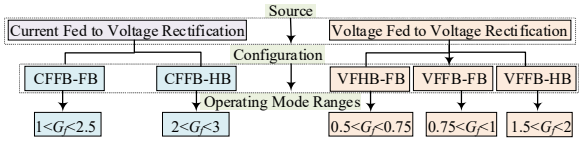

Fig. 2. Operating modes with current/voltage-fed (CF/VF) configuration topology morphing.

stresses, and selecting the best-performing operating modes enabled by the topology morphing control.

The paper is organized as follows. The advantages of using dual current-fed active clamped full-bridge converter with series resonance and synchronous rectification for wide voltage range applications are discussed in section II. The design and control aspects of the proposed converter are explained in section III, followed by the validation of the converter in section IV. The conclusions are provided in the last section.

II. Overview of Active Clamped Dual Current-Fed Bidirectional Converter

A. Overview of the Proposed Topology

The proposed configuration of an active clamped dual current-fed (ACDCF) bidirectional dc-dc converter contains active clamp circuits at input and output terminals and reconfigurable full-bridge (FB) switching cells connected to the resonant tank through the isolation transformer (refer to Fig. 1). The blocking capacitors are employed to block dc bias in transformer that can occur during asymmetrical control. They enable the reconfiguration of switching cells from FB to half-bridge (HB) [16]. In addition, the blocking capacitors and the resonant inductance form a series resonant tank. The series resonant inductance can be fully implemented as the transformer's leakage inductance, or a discrete inductor can be applied to satisfy the operational requirement of the converter. For ease of analysis, all the leakage and auxiliary inductance are represented by the equivalent resonant inductance at the secondary side of the transformer L_r. Thus, the resonant frequency can be represented as follows:

$$f_r = \frac{1}{(2\pi\sqrt{L_r C_r})} \tag{1}$$

where C_r represents the equivalent capacitor that includes the series capacitors at both sides of the transformer; it can be estimated by:

$$C_r = \frac{C_b C_s}{C_b + C_s} \tag{2}$$

Thanks to topology morphing (see Fig. 3), the converter can introduce a change in overall converter gain G_f through

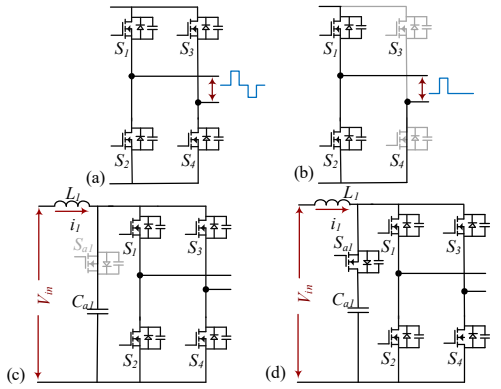

Fig. 3. Reconfiguration possibilities of switching cells through topology morphing control: (a) full-bridge inverter cell, (b) half-bridge inverter cell, (c) VF full-bridge inverter, and (d) CF active clamped full-bridge inverter.

reconfiguration of the switching cells in terms of topology type (FB or HB, see Fig. 3a,b), and configuration (VF or CF see Fig. 3c,d). This allows the converter to adapt its gain depending on the requirement.

The normalized forward voltage gain G_f can be characterized as follows:

$$G_f = {}^{V_{out}}/_{n \cdot V_{in}} = G_{XF} \cdot G_{SRC} \cdot G_{VR} \tag{3}$$

where G_{XF} is the gain of the input side switching cell ($X = C$ and $X = V$ represent the gain of the active clamped current-fed and the voltage-fed inverters, correspondingly), and G_{VR} represents the gain of the rectifier side. Only one active clamping circuit can be activated simultaneously, creating the topology configurations discussed in this section. The normalized gain of the series resonant stage designated by G_{SRC} depends on the modulation used to achieve buck voltage regulation in the VF topology configurations. Possible modulations were covered in the existing literature [18], [19].

Hence, the maximum feasible operating modes are shown in Fig. 2 and can be characterized based on the CF/VF inverter type operated at the input side. As a result, the following topology configurations are feasible: full-bridge inverter with full-bridge rectifier (FB-FB), full-bridge inverter with half-bridge rectifier (FB-HB), and half-bridge inverter with full-bridge rectifier (HB-FB) operating modes. It is worth mentioning that the topology is symmetrical, so its operation is similar for forward and backward power flow. Hence, only the forward power flow is considered in this paper.

B. Boost Operation of the Current-Fed (CF) Configurations

The CF configurations provide up to threefold normalized gain when switching from an FB to an HB (voltage doubler) rectifier. Hence, converter operation in the boost mode is always associated with using a CF inverter on the input side.

The CFFB-FB topology is controlled by the diagonal switches pair (S_1/S_4 and S_2/S_3) with complementary gating signals (see Fig. 4*a*). These gating signals have duty cycle D_p, while the gating signals of S_2 and S_3 switches are 180 out of phase to S_1 and S_4 switches. The minimum duty of the switches is always held above 50% to ensure the symmetrical overlap times between the top and bottom switch of the same leg. In contrast to VF converters, the overlap of control signals results in shoot-through states, which define the boost value.

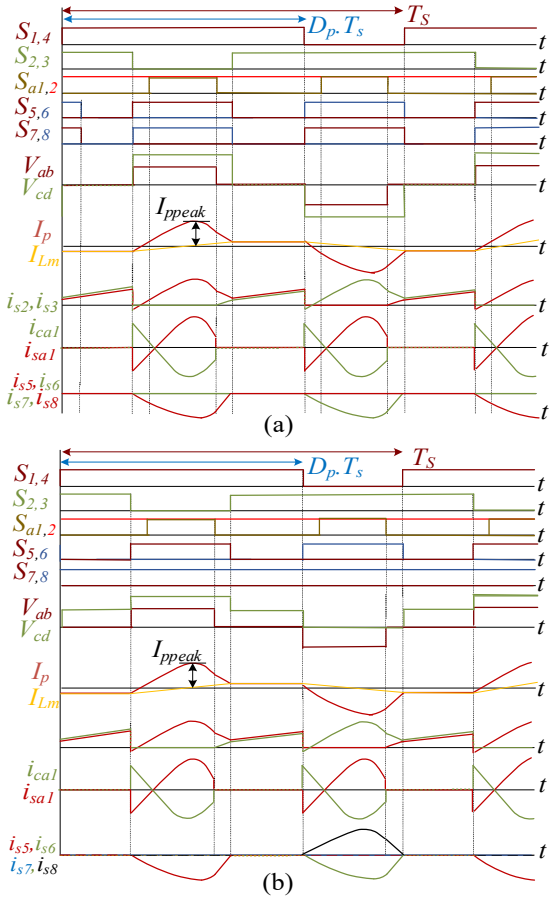

Fig. 4. Converter operation in the boost mode for configurations (a) CFFB-FB and (b) CFFB-HB configurations.

The auxiliary switches S_{a1} and S_{a2} are controlled in such a way that one turns on complimentary to the main switches of the inverter cell that feeds power to the isolation transformer, while the other is turned on continuously. Therefore, during forward power flow, S_5-S_8 are switched as synchronous rectifiers, while S_{a2} is turned on continuously to configure the output-side cell as a VF rectifier. At the same time, S_{a1} is controlled to provide the active clamping to the switches S_1-S_4 of the current-fed bridge. This represents the CFFB-FB configuration, with a current-fed full-bridge inverter on the primary side and a full-bridge VF rectifier on the secondary side. The active clamp switch has twice the switching frequency of the main switches. It clamps the voltage stress and assists in achieving the ZVS turn-on of the main switches [13]. The CFFB-FB topology can provide over twofold normalized dc gain. The operation of the primary side is otherwise comparable to a full bridge configuration. The respective voltage gain for CFFB-FB topology can be reproduced from [13], considering $G_{VR} = 1$ as follows:

$$G_f = G_{CF} = \frac{V_{out}}{n.V_{in}} = \frac{1}{2(1-D_p)} \tag{4}$$

Furthermore, the CFFB-HB configuration (Fig. 4*b*) can provide an additional voltage boost and thus has been considered. In this mode, the CFFB inverter is controlled by duty cycle D_p, similar to the CFFB-FB configuration. However, in this case, the rectifier cell is modified as an HB by turning off switch S_7 and turning on switch S_8 continuously, while switches S_5 and S_6 operate as synchronous rectifiers. The voltage gain of the CFFB-HB configuration is doubled due to the use of a voltage doubler ($G_{VR} = 2$):

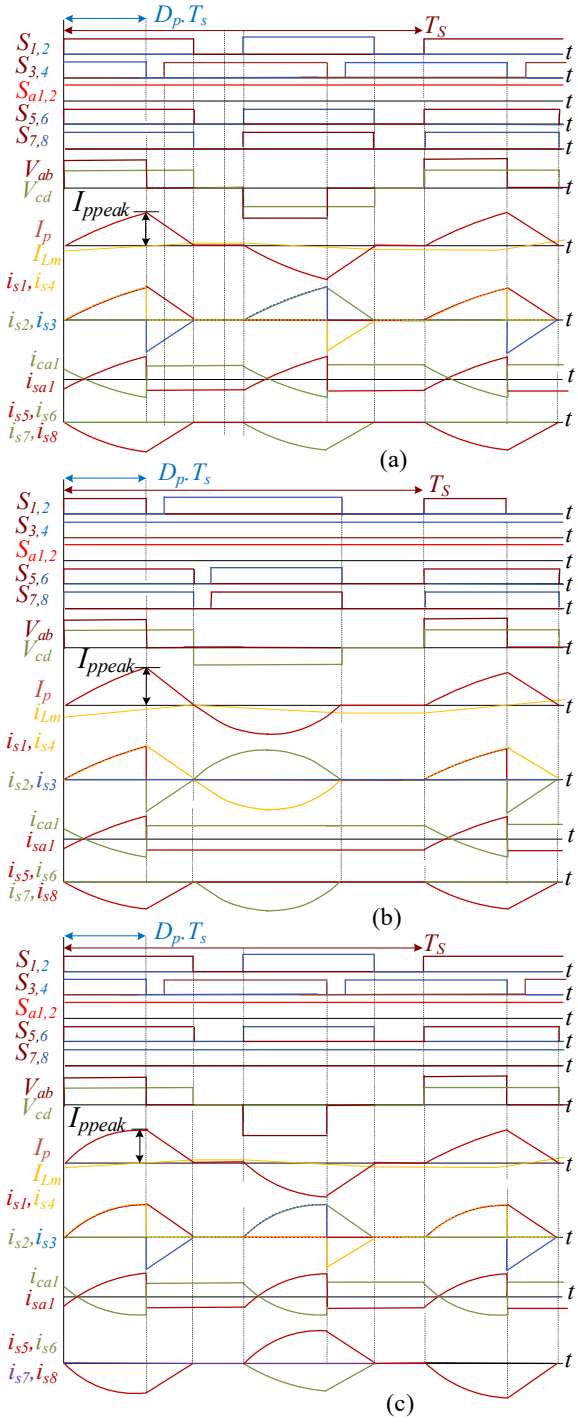

Fig. 5. Converter operation in buck mode configurations (a) VFFB-FB and (b) VFHB-FB, and boost mode in (c) VFFB-HB modes

$$G_f = G_{CF} = \frac{2.V_{out}}{n.V_{in}} = \frac{1}{(1-D_p)} \tag{5}$$

As the CF inverter performs voltage regulation, the overall gain G_f mainly depends on variations of G_{CF}. Moreover, the CFHB-FB configuration was considered redundant due to its low normalized dc gain and thus is not considered.

C. Buck Operation of the VF Configurations

The VF configurations are effective in buck mode operation (below the unity normalized gain) and thus can extend the regulation range for the current-fed converter. In VF configurations, both active clamp switches are turned on

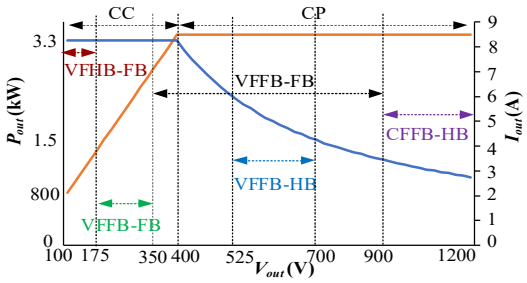

Fig. 6. A case-study safe operating area and corresponding distribution of the converter operating modes.

continuously to mimic the voltage-fed inverter and bridge rectifier with a capacitive filter. There are three possible configurations: VFHB with FB rectifier (VFHB-FB), VFFB with FB rectifier (VFFB-FB), and VFFB with HB rectifier (VFFB-HB). The derivations of the voltage gain of the converter can be found in [16].

In the VFFB-FB configuration (Fig. 5*a*), the switches S_1-S_4 control the normalized dc gain below unity with duty cycle D_p, representing the phase shift between the leading leg and lagging leg of the inverter bridge. Further, the secondary side witches S_5-S_8 are switched as synchronous rectifiers to reduce the conduction losses at the secondary-side FB. The respective voltage gain of the FBI-FBR configuration was deduced from [15] as follows:

$$G_f = \beta(0.25 - \alpha) + \sqrt{((\beta(\alpha - 0.25))^2 + 2\alpha\beta)}, \quad (6)$$

where

$$\alpha = C_r R_L f_{sw} \text{ and } \beta = 1 - \cos(\omega_r D_p / f_{sw}). \quad (7)$$

In the VFHB-FB configuration (Fig. 5*b*), only switch S_1 has been controlled with duty cycle D_p along with its complimentary switch S_2 with fixed duty cycle equivalent to a resonant half-cycle and reduced conduction time to improve the soft switching performance of the converter. The switch S_3 is turned off, and switch S_4 is turned on continuously to reconfigure the FB cell into HB. Switches S_5-S_8 are operated as synchronous rectifiers. The normalized dc gain of the converter for the HBI-FBR configuration can be expressed as follows:

$$G_f = 0.5(\beta(0.5 - \alpha) + \sqrt{((\beta(\alpha - 1))^2 + 4\alpha\beta)}). \quad (8)$$

The VFFB-HB and VFFB-FB topology configurations are similar in operation (see Fig. 5*c*). The buck operation is implemented by providing the phase shift D_p between switches S_1-S_2 and S_3-S_4. To implement an HB rectifier configuration, switches S_7 and S_8 are continuously turned off and on, correspondingly, while switches S_5 and S_6 operate in synchronous rectification mode. The voltage gain of the HBI-FBR configuration gets doubled due to the use of a voltage doubler rectifier ($G_{VR} = 2$) and can be expressed as follows:

$$G_f = \frac{1}{2}(\beta(1 - \alpha) + \sqrt{\beta^2(\alpha - 1)^2 + 8\alpha\beta}) \quad (9)$$

D. Redundant Modes

The CFHB-FB is disadvantageous for implementing boost operating mode as its normalized dc gain is similar to VF configurations. Similarly, the boost operations with a VF configuration are replaced by the CF configuration best suited to operate at normalized dc gains above the unity. Hence, these modes have not been considered.

III. Converter Design and Control

A. ACDCF Converter Design

The selection of major passive components of the ACDCF converter is briefly described in this section.

1) The boost inductors L_1 and L_2 can be designed using methodology from [12], as follows:

$$L_x = \frac{V_{in} \cdot (D_{pmax} - 0.5)}{\Delta I_x \cdot f_{sw}}\Big|_{x=1,2}, \quad (10)$$

where the maximum duty cycle $D_{pmax} = 0.85$ is based on the maximum gain required, f_{sw} is the switching frequency, and ΔI_x is the allowed current ripple of the x-th dc inductor.

2) The minimum value of the x-th (x=1,2) auxiliary capacitors, C_{ax}, is designed based on the capacitor peak resonant current I_{Caxp}, and permissible voltage ripple ΔV_{Cax}, (x=1,2) across it can be presented as:

$$C_{ax} = \frac{I_{Capx} \cdot \sqrt{2(1 - D_{pmax})/3}}{[4\pi \Delta V_{Cax} \cdot f_{sw}]}\Big|_{x=1,2} \quad (11)$$

3) Ideally, a large magnetizing inductance is always preferred to minimize the amplitude of the magnetizing current, which directly helps reduce conduction losses. In practice, the magnitude of the magnetizing current can be designed enough to discharge the output capacitances (C_{oss}) of the switches. Hence, the derived magnetizing inductance value can be expressed as follows.

$$L_m < \frac{T_{Dmax} \cdot n}{[16 \cdot C_{ossx} \cdot f_{sw}]}, \quad (12)$$

where T_{Dmax} is the max dead time between gate driving signals of the complementary devices in the buck mode.

4) The resonant inductance value in earlier analysis requires a larger value to limit the resonant current, but the proposed converter limits the current flow due to the inherent current-limiting nature of the current-fed converter during *CF-VF* operation. Hence, a maximum feasible value of the resonant inductor L_{rmax} can be derived based on the VFFB-FB operation of the proposed converter, as given in [16]:

$$L_{rmax} < \frac{V_{outmax} \cdot f_{sw}}{I_{2max} \cdot \omega_r^2}, \quad (13)$$

where V_{outmax} and I_{2max} represent the maximum output voltage and current of the VFFB-FB configuration, respectively, as defined by the safe operating area (refer to Fig. 6).

5) Blocking capacitors C_b should be high enough not to disturb the resonant frequency. They block the dc bias in the transformer current, while series resonant capacitor C_s should resonate with resonant inductance. Usually, the C_b is selected large enough in comparison to resonant capacitance, and it can be simply approximated from the fundamental relationship between resonant inductance and capacitance as follows:

$$C_s \approx \frac{1}{L_{rmax} \cdot \omega_r^2}. \quad (14)$$

B. Control Aspects

The proposed converter employs five modes for operating in a safe operating area. The distribution of the operating modes across the output voltage range is given in Fig. 6.

The proposed control method is presented in Fig. 7. In which mode selection block switches the converter state based on the voltage gain of the converter. A single control variable

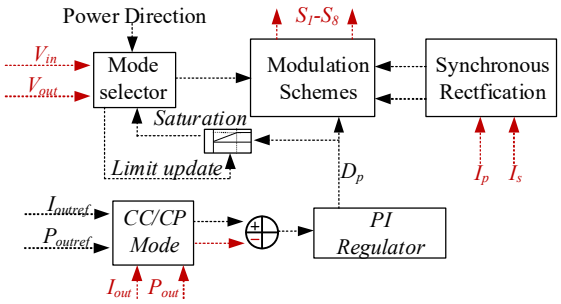

Fig. 7. Simplified control block diagram for ACDCF converter.

TABLE I. CONVERTER SPECIFICATIONS

Parameters	Symbols	Values
Input voltage	V_{in}	350 V
Output voltage	V_{out}	150-1000 V
Switching frequency	f_{sw}	100 kHz
Turn ratio	n	1:1
Blocking capacitor primary side	C_b	15 µf
Series capacitor secondary side	C_s	309 nf
Series resonant inductance	L_r	7.5 µf
Input inductor	L_1	100 µH
Output inductor	L_2	100 µH
Power Range	P_{out}	0.5-3.3 kW
Max output current at low V_{out}	I_{omax}	8.25 A

controls this converter, and each mode has its duty cycle D_p range tailored using different saturation limits for each mode. Further, the duty cycle is regulated using a PI controller to achieve the constant output current or power (CC/CP). A synchronous rectifier block is also connected to the modulation block for the gating signal of synchronous switches using transformer primary I_p and secondary I_s currents. Also, the whole control block can operate in reverse power based on the user input to the power direction block.

IV. VALIDATION OF PROPOSED ACDCF CONVERTER

The converter specifications considered for simulation work are listed in Table I. The simulation results shown in Fig. 8 to Fig. 12 ensure the soft switching capabilities of the converter in each mode.

A. Simulation of the converter in different modes

PSIM software was used to validate the converter operation predicted theoretically for the buck operation of VF configurations and the boost operation of CF configurations.

1) *Buck operation with VF configurations*

For VFHB-FB buck mode, the modulation scheme described in Fig. 5*b* has been validated in simulation and shown in Fig. 8. For VFFB-HB buck mode, the modulation scheme described in Fig. 5*c* has been validated in simulation and shown in Fig. 9. For VFFB-FB buck mode, the modulation scheme described in Fig. 5*a* has been validated in simulation and shown in Fig. 10.

2) *Boost operation with CF configurations*

For CFFB-FB mode, the modulation scheme described in Fig. 4*a* has been validated in simulation and shown in Fig. 11. For CFFB-HB mode, the modulation scheme described in Fig. 4*b* has been validated in simulation and shown in Fig. 12.

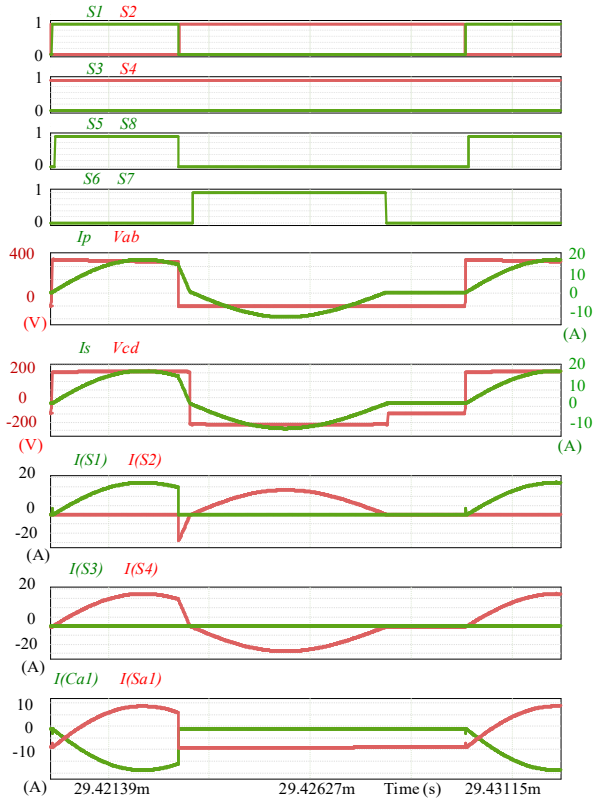

Fig. 8. Simulation waveform for VFHB-FB buck mode.

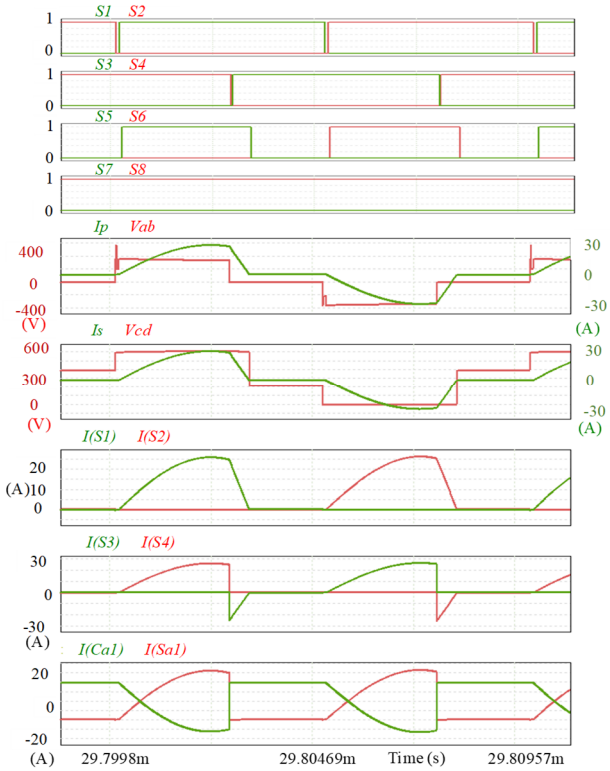

Fig. 9. Simulation waveform for VFFB-HB buck mode

B. System Characteristics

Data points from the simulation of all five modes have been presented in graphical form to summarize the converter performance metrics in Fig. 13. Fig. 13*a* shows the current stress ratio ($CSR = I_{ppeak}/I_{prms}$) versus the duty cycle, which

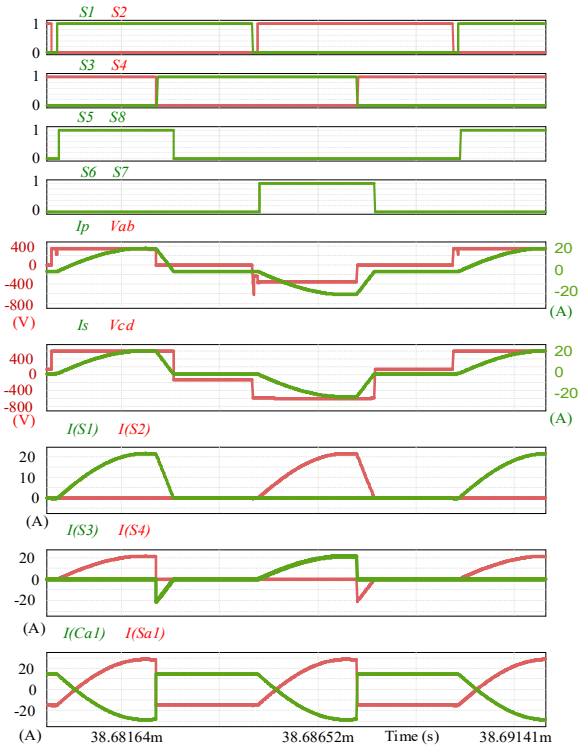

Fig. 10. Simulation waveform for VFFB-FB mode.

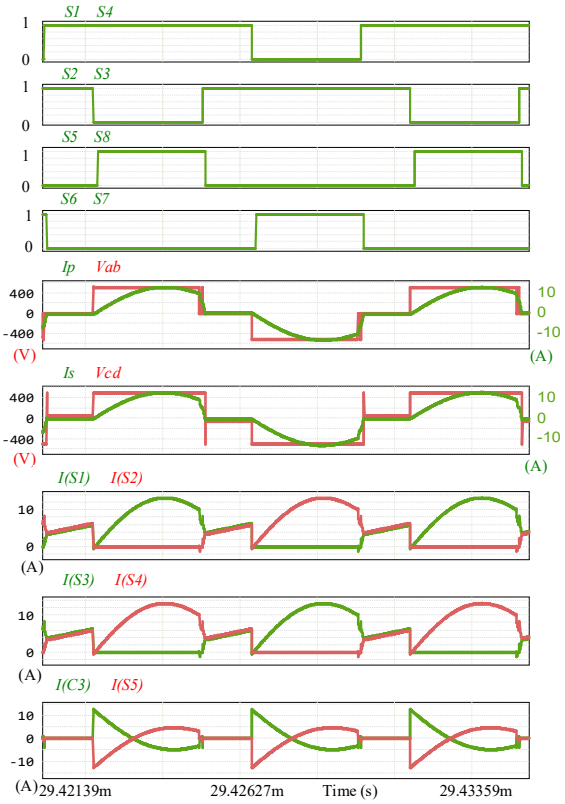

Fig. 11. Simulation waveform for CFFB-FB mode.

expectedly shows the minimal *CSR* at nearly 50% duty. The CFFB-HB configuration has minimum current stress for similar duty cycle values but has higher I_p than the CFFB-FB configuration, which may lead to higher losses.

Hence, the CFFB-FB configuration is considered to be better for converter operation at normalized dc gains between 1.0 and 2.5, while the CFFB-HB configuration is optimal for

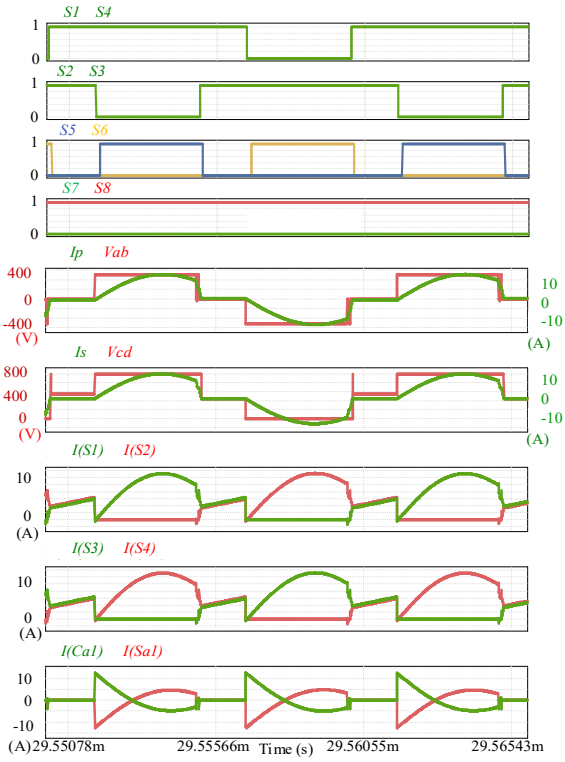

Fig. 12. Simulation waveform for CFFB-HB mode.

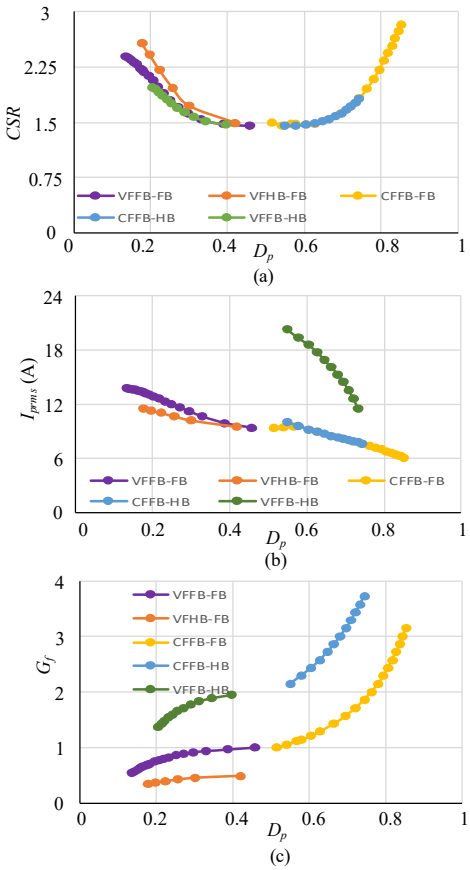

Fig. 13. Converter key performance indicators plotted versus the duty cycle D_p for all five operating modes (considering the safe operating area): (a) *CSR*, (b) transformer rms current I_{prms}, and (c) the normalized dc voltage gain.

normalized dc gains above 2.5, as shown in Fig. 13*b*. In Fig. 13*c*, the overall voltage gain G_f has been plotted versus the duty cycle to show the control range of the converter. The

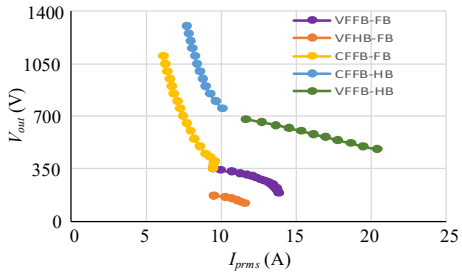

Fig. 14. Converter output voltage plotted versus the transformer rms current I_{prms} for all five operating modes and considering the safe operating area.

operating boundaries between the converter configurations can be defined based on the gain range for a particular mode. Fig. 14 shows the dependencies between the output voltage and transformer rms current to prove the converter's balanced performance over a wide range of output voltages. The transformer rms current was found to be below double the maximum output current.

V. Conclusion

Due to its symmetrical topology, the proposed ACDCF converter has an inherent bidirectional power flow feature. This converter is intended to operate in two configurations (voltage-fed and current-fed) with five overall modes enabled by the topology morphing control. This allows the converter to operate in a wide range of output voltages without significantly increasing the transformer rms current. Various modes have been analyzed to explain the converter's operating principle based on the topology morphing control. The simulation results provided for each operating mode cover the overall voltage gain range (0.4-3). The control duty cycle could be constrained to the range of acceptable current stresses owing to topology reconfigurations. The transformer rms current is always below double the maximum charging current for the entire operating range. Similarly, the CSR is limited to 2.5 times for different output voltages, visualizing the converter boundary limits for various duty cycles and gain ranges. The proposed topology performed very well for the noticeably wide voltage gain range. The future work will be validated using an experimental hardware setup.

Acknowledgments

This research was supported in part by the Estonian Research Council under the grant PRG2055, in part by the Estonian Centre of Excellence in Energy Efficiency, ENER, funded by the Estonian Ministry of Education and Research under Grant TK230, and in part by the European Union's Horizon Europe research and innovation programme under grant agreement no. 101136131. Views and opinions expressed in this document are those of the authors only and do not necessarily reflect those of the European Union or the European Climate, Infrastructure and Environment Executive Agency (CINEA). Neither the European Union nor the granting authority can be held responsible for them.

References

[1] K. Wang, C. Y. Lin, L. Zhu, D. Qu, F. C. Lee, and J. S. Lai, "Bi-directional DC to DC converters for fuel cell systems," *Power Electronics in Transportation (Cat. No.98TH8349)*, IEEE, pp. 47–51, 1998.

[2] J. Gallardo-Lozano, E. Romero-Cadaval, V. Miñambres-Marcos, D. Vinnikov, T. Jalakas and H. Hõimoja, "Grid reactive power compensation by using electric vehicles," 2014 Electric Power Quality and Supply Reliability Conference (PQ), Rakvere, Estonia, 2014, pp. 19-24.

[3] X. Pan, H. Li, Y. Liu, T. Zhao, C. Ju, and A. K. Rathore, "An Overview and Comprehensive Comparative Evaluation of Current-Fed-Isolated-Bidirectional DC/DC Converter," *IEEE Trans Power Electron*, vol. 35, no. 3, pp. 2737–2763, 2020.

[4] Y. Zhang, L. Ding, N. Hou, and Y. Li, "A Dual-Current-Fed Dual-Active-Bridge DC/DC Converter With High-Frequency Current-Ripple-Friendly Ports," *IEEE Trans Power Electron*, vol. 37, no. 12, pp. 15084–15098, 2022.

[5] A. Blinov, R. Kosenko, A. Chub, and D. Vinnikov, "Bidirectional Soft Switching Current Source DC-DC Converter for Residential DC Microgrids," in *IECON 2018 - 44th Annual Conference of the IEEE Industrial Electronics Society*, IEEE, 2018, pp. 6059–6064.

[6] P. Xuewei and A. K. Rathore, "Novel bidirectional snubberless soft-switching naturally clamped zero current commutated current-fed dual active bridge (CFDAB) converter for fuel cell vehicles," in *2013 IEEE Energy Conversion Congress and Exposition*, IEEE, 2013, pp. 1894–1901.

[7] A. Chub, R. Kosenko, and A. Blinov, "Zero-voltage switching galvanically isolated current-fed full-bridge DC-DC converter," in *2016 10th International Conference on Compatibility, Power Electronics and Power Engineering (CPE-POWERENG)*, IEEE, 2016, pp. 455–459.

[8] Y. Chen, R. Ota, and N. Hoshi, "Current-Fed Dual Active Bridge Converter With Asymmetric Three-Phase Transformer," *IEEE Open Journal of Power Electronics*, vol. 5, pp. 648–663, 2024.

[9] Y. Zhang, Z. Wang, Y. W. Li, N. Hou, and M. Cheng, "Decoupled Dual-PWM Control for Naturally Commutated Current-Fed Dual-Active-Bridge DC/DC Converter," *IEEE J Emerg Sel Top Power Electron*, vol. 8, no. 4, pp. 4246–4259, 2020.

[10] B. Zhu, H. Wang, Y. Zhang, and S. Chen, "Buck-Based Active-Clamp Circuit for Current-Fed Isolated DC–DC Converters," *IEEE Trans Power Electron*, vol. 37, no. 4, pp. 4337–4345, 2022.

[11] K.-C. Tseng, S.-Y. Chang, and C.-A. Cheng, "Novel Isolated Bidirectional Interleaved Converter for Renewable Energy Applications," *IEEE Transactions on Industrial Electronics*, vol. 66, no. 12, pp. 9278–9287, Dec. 2019.

[12] P. Xuewei and A. K. Rathore, "Bidirectional naturally clamped soft-switching current-fed push-pull DC/DC converter," in *IECON 2015 - 41st Annual Conference of the IEEE Industrial Electronics Society*, IEEE, 2015, pp. 4253–4258.

[13] P. U R and A. K. Rathore, "Extended Range ZVS Active-Clamped Current-Fed Full-Bridge Isolated DC/DC Converter for Fuel Cell Applications: Analysis, Design, and Experimental Results," *IEEE Transactions on Industrial Electronics*, vol. 60, no. 7, pp. 2661–2672, 2013.

[14] S. Bal, D. B. Yelaverthi, A. K. Rathore, and D. Srinivasan, "Improved Modulation Strategy Using Dual Phase Shift Modulation for Active Commutated Current-Fed Dual Active Bridge," *IEEE Trans Power Electron*, vol. 33, no. 9, pp. 7359–7375, Sep. 2018.

[15] P. Xuewei and A. K. Rathore, "Naturally Clamped Soft-Switching Current-Fed Three-Phase Bidirectional DC/DC Converter," *IEEE Transactions on Industrial Electronics*, vol. 62, no. 5, pp. 3316–3324, May 2015.

[16] V. Sidorov, A. Chub, and D. Vinnikov, "Bidirectional Isolated Hexamode DC–DC Converter," *IEEE Trans Power Electron*, vol. 37, no. 10, pp. 12264–12278, Oct. 2022.

[17] V. Sidorov, A. Chub, D. Vinnikov and F. Z. Peng, "Survey of Topology Morphing Control Techniques for Performance Enhancement of Galvanically Isolated DC-DC Converters," *IEEE Open J. of the Ind.l Electron. Soc.*, vol. 3, pp. 751-777, 2022.

[18] V. Sidorov, A. Chub, and D. Vinnikov, "Topology Morphing Control with Soft Transients for Multimode Series Resonant DC-DC Converter," in *2021 IEEE 22nd International Conference of Young Professionals in Electron Devices and Materials (EDM)*, IEEE, Jun. 2021, pp. 331–336.

[19] V. Sidorov, A. Chub, and D. Vinnikov, "Efficiency Improvement of Step-Up Series Resonant DC-DC Converter in Buck Operating Mode," in *2020 IEEE 61th International Scientific Conference on Power and Electrical Engineering of Riga Technical University (RTUCON)*, IEEE, Nov. 2020, pp. 1–6.

[20] O. Korkh, A. Blinov, D. Vinnikov, and A. Chub, "Review of Isolated Matrix Inverters: Topologies, Modulation Methods and Applications," *Energies* 2020, 13, p. 2394.